Acta Materialia 105 (2016) 155–164

Contents lists available at ScienceDirect

Acta Materialia

journal homepage: www.elsevier.com/locate/actamat

Full length article

Exploring bainite formation kinetics distinguishing grain-boundary and autocatalytic nucleation in high and low-Si steels

Ashwath M. Ravi*, Jilt Sietsma, Maria J. Santofimia

Department of Materials Science and Engineering, Delft University of Technology, Mekelweg 2, Delft, 2628 CD, The Netherlands

ARTICLE INFO

Article history:
Received 14 April 2015
Received in revised form
4 November 2015
Accepted 21 November 2015
Available online 24 December 2015

Keywords:
Bainite
Kinetics
Nucleation
Isothermal heat treatments

ABSTRACT

Bainite formation in steels begins with nucleation of bainitic ferrite at austenite grain boundaries (γ/γ interfaces). This leads to creation of bainitic ferrite/austenite interfaces (α/γ interfaces). Bainite formation continues through autocatalysis with nucleation of bainitic ferrite at these newly created α/γ interfaces. The displacive theory of bainite formation suggests that the formation of bainitic ferrite is accompanied by carbon enrichment of surrounding austenite. This carbon enrichment generally leads to carbide precipitation unless such a reaction is thermodynamically or kinetically unfavourable. Each bainitic ferrite nucleation event is governed by an activation energy. Depending upon the interface at which nucleation occurs, a specific activation energy would be related to a specific nucleation mechanism. On the basis of this concept, a model has been developed to understand the kinetics of bainite formation during isothermal treatments. This model is derived under the assumptions of displacive mechanism of bainite formation. The fitting parameters used in this model are physical entities related to nucleation and microstructural dimensions. The model is designed in such a way that the carbon redistribution during bainite formation is accounted for, leading to prediction of transformation kinetics both with and without of carbide precipitation during bainite formation. Furthermore, the model is validated using two different sets of kinetic data published in the literature.

1. Introduction

Bainite was discovered as an 'acicular, dark-etching aggregate' nearly eight decades ago [1,2]. Over the years, the research work done in the field of bainite is immense [3–7]. Bainite consists of sheaves of bainitic ferrite separated by untransformed austenite, martensite or cementite. Each bainitic sheaf is composed of a cluster of sub-units which are connected in three dimensions [8]. Due to the complexity of its formation mechanism, even a qualitative theory to explain the bainite formation still remains a subject of controversy [4,9,10]. One "school of thought" advocates a diffusion-controlled transformation where bainitic growth occurs by a diffusional 'ledge' mechanism while the other suggests that the bainite reaction is a displacive and diffusionless transformation [4]. Both "schools" have proposed different models to predict the transformation kinetics based on their own assumptions of bainite formation [11–16].

Bainite formation begins at austenite grain boundaries. This bainite formation, at the initial stages of transformation, leads to an increase in the number density of nucleation sites. Bainite formation continues autocatalytically at these newly created nucleation sites. Santofimia et al. [17] reviewed and evaluated several kinetic models which are based on assumptions of displacive theory of bainite formation. Since displacive theory for bainite formation assumes that the rate of bainite formation is driven by the rate of bainitic ferrite nucleation, most of the models are based on nucleation kinetics. It is evident from the review in Ref. [17] that the overall structure for determining the rate of bainite formation is consistent among various models. Santofimia et al. [17] commented that the models mostly vary only in the manner in which the nucleation rate is calculated. With the help of their review, some of the major shortcomings of the existing models can be identified.

Most of the existing nucleation based models developed using the displacive mechanism of bainite formation use several empirical constants to account for the number density of grain-boundary nucleation sites and the number density of autocatalytic nucleation sites [17]. However, the physical significance of the values obtained for the empirical constants is still unclear [18]. Although some models describe the autocatalytic nucleation using other means,

* Corresponding author.
E-mail addresses: A.M.Ravi@tudelft.nl (A.M. Ravi), J.Sietsma@tudelft.nl (J. Sietsma), M.J.SantofimiaNavarro@tudelft.nl (M.J. Santofimia).

http://dx.doi.org/10.1016/j.actamat.2015.11.044

such as geometrical conception of the transformation [14] and with the help of prior austenite grain size [19], they still use empirical constants to calculate the grain-boundary nucleation kinetics.

Furthermore, in case of steels that are lean in silicon, these existing models fail to properly calculate of the maximum volume fraction of bainite formed during transformation [17]. According to the displacive theory of bainite transformation, the formation of bainitic ferrite from austenite is accompanied by a subsequent partitioning of carbon into surrounding austenite matrix [8]. This leads to a carbon enrichment of austenite during the course of the transformation. Depending on the chemical composition of the steel, the degree of carbon enrichment of austenite can vary. In lean-silicon steels, the degree of carbon enrichment is negligible due to the precipitation of carbides during bainite formation. Most existing models do not account for this variable degree of enrichment which sometimes results in an underestimation of the maximum volume fraction bainite. Such an underestimation will lead to an improper prediction of the bainite formation kinetics.

In order to tackle the problem of predicting the kinetics of isothermal bainite formation in lean-silicon steels, Van Bohemen and Sietsma [15] developed a kinetic model based on nucleation kinetics. This model was developed using the concepts of displacive theory of bainite and martensite formation. Unlike previous models where several empirical constants were used, Van Bohemen and Sietsma used physical parameters to calculate the number density of grain-boundary nucleation sites. Since this model does not predict the incomplete reaction phenomenon which is exhibited by high silicon steels, Van Bohemen and Hanlon [16] proposed a modified version of the Van Bohemen and Sietsma model [15] for this purpose.

However, both Van Bohemen and Sietsma model [15] and Van Bohemen and Hanlon model [16] do not account for the condition that diffusionless growth of bainite can occur only when the transformation temperature is below a certain thermodynamic limit as proposed by Ref. [20]. According to the displacive approach of the bainite transformation, it has been suggested that the displacive formation of bainite can proceed if and only if the following conditions,

$$\Delta G_m < G_N; \quad \text{where} \quad \Delta G_m = G_m^{\alpha} - G_m^{\gamma} \tag{1}$$

$$\Delta G^{\gamma\rightarrow\alpha} < -G_{SB}; \quad \text{where} \quad \Delta G^{\gamma\rightarrow\alpha} = G^{\alpha} - G^{\gamma} \tag{2}$$

are satisfied [20]. $\Delta G^{\gamma\rightarrow\alpha}$ represents the free energy change during bainite formation. G^{α} and G^{γ} give the ferrite free energy and austenite free energy respectively, when both the composition of ferrite and of austenite is equal to the composition of interest. ΔG_m is the maximum driving force for nucleation. It is the greatest possible reduction in free energy that can be achieved during formation of a ferrite nucleus such that the composition of surrounding austenite matrix remains unaffected. It is calculated using parallel tangent construction. G_m^{α} and G_m^{γ} give the ferrite free energy and austenite free energy when this condition of maximum free energy reduction is achieved. G_N is the universal nucleation function [3]. G_{SB} is the stored energy of bainite which is usually considered to be 400 J mol^{-1} [20]. Eq. (1) indicates that a bainite nucleus can develop only at temperatures where ΔG_m is more negative than G_N. The temperature at which $\Delta G_m = G_N$ is called the T_h temperature. Furthermore, a diffusionless growth of bainite can occur only if Eq. (2) is satisfied. The maximum temperature below which diffusionless growth of bainite can occur ($\Delta G^{\gamma\rightarrow\alpha} = -G_{SB}$) is called the T_0' temperature [8]. Therefore, according to Eq. (1) and Eq. (2), bainite formation can occur only when the isothermal transformation temperature is below both T_h and T_0' temperature.

Both T_h and T_0' temperatures decrease with increasing carbon enrichment of austenite during the course of bainite formation. Generally, it is observed that the T_0' temperature decreases at a much faster rate with increasing carbon enrichment compared to the T_h temperature. When, during the transformation, either T_h or T_0' temperature becomes equal to the transformation temperature, the bainite reaction will terminate and an incomplete reaction phenomenon will be exhibited. The nucleation rate at this point is equal to 0. Van Bohemen and Sietsma model and Van Bohemen and Hanlon model only consider the dependence of the nucleation rate on the T_h temperature and not on the T_0' temperature. Its effects would not be significant in the prediction of bainite kinetics in lean silicon steels due to negligible effective carbon enrichment of austenite during transformation. However without such a dependence, in case of high silicon steels, the nucleation rate at the end of the transformation may not always reach 0. This implies that the model predicts further bainite formation which is physically unrealistic.

In this work, a unified model to predict the kinetics of isothermal bainite formation regardless of the degree of carbon enrichment of austenite is proposed. In an attempt to better treat the autocatalytic nucleation, a physically based approach considering the difference in the activation energy for grain-boundary nucleation and for autocatalytic nucleation is proposed here. The model is derived under the assumptions given by the displacive theory of bainite formation and draws inspiration from previously proposed models [15,21]. The model fitting parameters are used in such a way that its physical significance can be interpreted.

2. The model

2.1. Nucleation rate

Bainitic ferrite sub-units may nucleate either at austenite grain boundaries (γ/γ interface) or at the interphase boundary of a previously nucleated sub-unit (α/γ interface). The latter is interpreted as autocatalytic bainite nucleation [8]. The total nucleation rate during bainite formation from a fully austenitic phase, dN/dt, can be given as

$$\frac{dN}{dt} = \left(\frac{dN}{dt}\right)_G + \left(\frac{dN}{dt}\right)_A \tag{3}$$

where $(dN/dt)_G$ is the nucleation rate per unit volume due to nucleation at austenite grain boundaries and $(dN/dt)_A$ is the nucleation rate per unit volume due to autocatalytic nucleation.

It is generally accepted that bainite nucleation is a thermally activated process [3]. According to displacive theory of bainite formation, two types of atomic processes may require thermal activation [3,20,22,23]. Firstly, the mechanism of bainite nucleation involves dissociation of certain dislocation defects which are already present in the austenite phase. Secondly, in order to create the necessary driving force for nucleation, carbon must partition from the bainitic nucleus into the surrounding austenite matrix. Both these processes require thermal activation. The nucleation rate is usually expressed as an exponential function of the temperature [17]. Using this approach, the nucleation rate due to grain-boundary nucleation can be written as

$$\left(\frac{dN}{dt}\right)_G = \frac{kT}{h} N_{tG} \exp\left(-\frac{Q_G^*}{kT}\right) \tag{4}$$

where k is the Boltzmann's constant, h is the Planck's constant, N_{tG} is the number density of potential grain-boundary nucleation sites at given time t, Q_G^* is the activation energy for grain-boundary nucleation and T is the isothermal transformation temperature.

After nucleation at the austenite grain boundaries, the bainite formation continues through autocatalytic bainite nucleation to form the bainitic sheaves. Studies have been conducted to understand the lengthening rate of bainitic sheaves [3,24,25]. These studies indicate that the lengthening of bainitic sheaves is a time dependent process. Furthermore, it was pointed out that the growth of the bainitic sub-units is much faster than the growth of the sheaves [26]. This suggests that the autocatalytic nucleation, which is necessary for the growth of the sheaves, is also a time dependent process and requires thermal activation.

The autocatalytic nucleation is accounted for in Refs. [15–17] with the help of autocatalytic parameter. This parameter is analogous to the autocatalytic factor used to describe the kinetics of isothermal martensite transformation in Refs. [27,28]. In these papers, the autocatalytic parameter is treated as an empirical dimensionless coefficient [12,17]. However, since the autocatalytic nucleation is a thermally activated nucleation event, its nucleation rate may also be expressed similarly as Eq (4), by

$$\left(\frac{dN}{dt}\right)_A = \frac{kT}{h} N_{tA} \exp\left(-\frac{Q_A^*}{kT}\right) \tag{5}$$

N_{tA} is the number density of potential autocatalytic nucleation sites at given time t and Q_A^* is the activation energy for autocatalytic nucleation. Q_A^* will be different from Q_G^* due to difference in the type of interface at which the nucleation takes place. Q_A^* can be related to Q_G^* by

$$Q_A^* = Q_G^* - \Delta Q^* \tag{6}$$

where ΔQ^* is the difference in the activation energy for grain-boundary nucleation and autocatalytic nucleation.

Such an interpretation for the autocatalytic nucleation rate would form the physical basis for the autocatalytic parameter as will be shown later in the paper.

2.2. Potential nucleation sites

The nucleation rate in Eq. (4) and Eq. (5) is expressed with a Boltzmann factor which gives the probability of successful nucleation events. In order to estimate the number of successful nucleation events, it is important to quantify, besides this probability, the number of potential nucleation sites. Van Bohemen and Sietsma [15] calculated the total number density of potential nucleation sites initially present in austenite (before bainite formation begins) using the principles of models for martensite formation. Magee's work [28] on athermal martensite nucleation suggests that the total number of martensitic plates per unit volume, N_m, that form during martensite formation at a particular temperature can be expressed as

$$N_m = \frac{m}{\overline{V}}(M_s - T) \tag{7}$$

where $\overline{V}$ is the average volume of a martensitic plate and M_s is the martensite start temperature. The number of nucleation events would be equal to the number of martensitic plates that form. Therefore, m is the proportionality constant between number of martensite nucleation sites and the degree of undercooling. It can be postulated that at a given undercooling below a critical temperature, the number of potential martensitic type nucleation events can be expressed using an equation similar to Eq. (7). With this assumption, the number of potential nucleation sites for grain-boundary nucleation during bainite formation can be given by

$$N_{tG} = \frac{b_G}{V_b}(T_h - T) \tag{8}$$

where b_G is a parameter for grain-boundary nucleation during bainite formation and V_b is the volume of a bainitic ferrite sub-unit.

b_G parameter acts as a proportionality constant between the number of nucleation sites and the degree of undercooling with respect to T_h temperature. This parameter is analogous to the fitting parameter, α, in the Koistinen and Marburger equation [29] as well as to the parameter, m, suggested in the work of Magee [28].

It must be noted that Eq. (8) gives the density of potential nucleation sites while the Eq. (7) gives the number density of nucleation events. This is because the bainite nucleation requires a thermal activation, similar to isothermal martensite nucleation [20,21], while athermal martensite formation does not need a thermal activation for nucleation. Therefore, the number density of nucleation events would be equal to the number density of nucleation sites during athermal martensite formation since the probability of successful nucleation given by the Boltzmann factor is equal to 1. However, during bainite formation, the number density of nucleation events would be much lower than the number density of potential nucleation sites. Eq. (8) gives maximum number density of possible bainite nucleation events. It is assumed that this maximum number density of possible nucleation events is numerically equal to the number density of potential nucleation sites. Eq. (8) in combination with Eq. (4) gives the actual number density of successful grain-boundary nucleation events during bainite formation.

Van Bohemen and Sietsma [15] pointed out that one of the key differences between martensite nucleation and bainite nucleation is that the density of pre-existing defects for martensite nucleation is independent of the prior austenization while the number density of γ/γ interfaces play an important role in bainite nucleation. Therefore, with the help of Van Bohemen and Sietsma [15] approach, b_G parameter can be given in relation to m if the effect of γ/γ interfaces is included. The density of available γ/γ interfaces depends on the fraction of remaining available austenite and the grain size of austenite. Thus, b_G parameter can be written as

$$b_G = \frac{Z\delta}{d} m f_\gamma \tag{9}$$

where Z is a geometrical factor, δ is the effective thickness of an austenite boundary, d is the prior austenite grain size and f_γ is the volume fraction of remaining available austenite.

The factor $Z\delta/d$ accounts for the austenite grain boundary area per unit volume. For spherical austenite grains, Z would to be equal to 6. Van Bohemen and Sietsma proposed that δ is the effective thickness of the austenite grain boundary. The effective thickness of an austenite grain boundary is defined here as the atomic layers of a grain in the grain boundary region which can be involved in grain-boundary nucleation. It is assumed only a few of outermost atomic layers in a grain participate in the nucleation process and therefore δ is considered to be equal to 1 nm, equivalent to 2 atomic layers in each grain.

The remaining available austenite, f_γ, is defined in this work as the fraction of austenite still remaining in which bainite formation can occur. This may not be equal to the total fraction of remaining austenite due to the “incomplete reaction phenomenon” exhibited during bainite formation [4]. Further description of f_γ is given in Section 2.4.

With the help of Eq. (8) and Eq. (9), N_{tG} as a function of volume fraction of bainite, f, may be schematically represented according to Fig. 1.

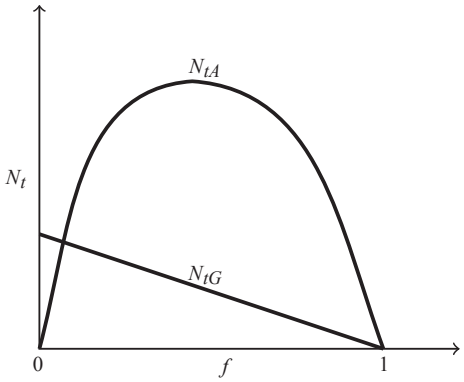

Fig. 1. Schematic representation of potential nucleation sites as function of volume fraction of bainite.

The number of potential autocatalytic nucleation sites can be derived similarly. Equivalent to Eq. (8), it is written as

$$N_{tA} = \frac{b_A}{V_b}(T_h - T) \tag{10}$$

where b_A is a parameter for autocatalytic nucleation during bainite formation.

The b_A parameter is different compared to b_G parameter since the density of potential autocatalytic nucleation sites depends on the density of available α/γ interfaces. The density of available α/γ interfaces depends on both the fraction of bainite formed and the fraction of remaining available austenite. Assuming that the nucleation events are random, the number density of potential autocatalytic nucleation sites would be proportional to the surface area of the α/γ interface (Fig. 1).

The density of available α/γ interfaces also depends on the density of γ/γ interfaces since grain-boundary nucleation is a precursor for autocatalytic nucleation. If the austenite grain size is small, there are more grain-boundary nucleation events due to increased number density of γ/γ interfaces. Grain-boundary nucleation events lead to the creation of α/γ interfaces and therefore the kinetics of grain-boundary nucleation events influences the rate at which α/γ interfaces form. Assuming that the volume of bainitic ferrite sub-units is constant during bainite formation at a constant temperature, greater number of grain-boundary nucleation events leads to higher density of α/γ interfaces within a given time. Thus, b_A parameter also depends on the number density of γ/γ interfaces ($Z\delta/d$) and it can be written as a function of m by

$$b_A = \frac{Z\delta}{d} m f_\gamma f \tag{11}$$

where f is the volume fraction of bainite formed.

The potential number density of nucleation sites is also affected by the size of the bainitic sub-units. As the size of the sub-units decreases, the density of potential nucleation sites increases. Additionally, the size of the sub-units also affect the remaining available austenite in which subsequent nucleation can take place.

Such size effects are incorporated into the model in two ways. Firstly, the number density of potential grain-boundary and autocatalytic nucleation sites are calculated per unit volume of bainite formed (Eq. (8) and Eq. (10)). Most of the existing kinetic models for bainite formation developed using the displacive mechanism of bainite formation use a fitting parameter to define the number density of potential nucleation sites [17]. Van Bohemen et al. argue that this could lead to an imprecise treatment of the potential nucleation sites [15]. Considering the number density of potential nucleation sites as a function of the volume of the bainitic sub-unit is a more physically rigorous approach. Furthermore, it reduces the number of fitting parameters required for the model as shown in Ref. [15]. Secondly, the number density of potential grain-boundary and autocatalytic nucleation sites are calculated as a function of volume fraction of bainite formed, f. Since the volume fraction of bainite formed due to each nucleation event depends on the size of the bainitic sub-unit, such a formulation automatically includes the size effects bainitic sub-units on the remaining available austenite.

It should be observed that as the equations for number of potential nucleation sites already track the changes in the density of available interfaces, the extended volume concept of the JMAK formulation is not used in this work. A similar approach has been used in earlier models [12,15].

2.3. Carbon enrichment

Carbon enrichment of austenite during isothermal formation of bainite heavily influences its kinetics as well as the eventual fraction of bainite which forms during transformation. Generally, carbon enrichment of austenite leads to precipitation of carbides which implies that the effective carbon enrichment of austenite is negligible [15]. However, in steels with high silicon or aluminium content, the carbide precipitation is kinetically suppressed, leading to significant carbon enrichment of austenite during transformation [30]. The transformation becomes slower as it progresses, since the effective activation energy increases and the effective undercooling thus decreases. In order to account for the effect of carbon enrichment, the following assumptions are made.

1. Mass balance of carbon exists. Therefore, the carbon content in austenite, X_γ, can be expressed as a function of fraction of bainite formed, the carbon content in bainite X_b and bulk carbon content $\overline{X}$, according to

$$X_\gamma = \frac{(\overline{X} - fX_b)}{(1-f)}. \tag{12}$$

2. T_h decreases linearly with the increase of carbon concentration in austenite during transformation. With the use of Eq. (12), T_h can be expressed as

$$T_h = T_{h\overline{X}} - C_1 \frac{f(\overline{X} - X_b)}{(1-f)}. \tag{13}$$

$T_{h\overline{X}}$ is the T_h temperature at the beginning of the transformation ($f = 0$, $X_\gamma = \overline{X}$) and C_1 is a proportionality constant relating T_h and carbon content.

3. It is assumed that the carbon-enrichment dependent factors affect the grain-boundary nucleation and autocatalytic nucleation equally during bainite formation. Therefore, ΔQ^* (Eq. (6)) is constant during transformation.

X_b accounts for all the carbon which does not participate in the carbon enrichment of austenite. This implies that X_b accounts for the carbon in bainitic ferrite, in any carbides present as well as any carbon that has been lost to “carbon trapping”. Depending on the degree of carbon redistribution and carbide formation, the value of X_b can vary between 0 and $\overline{X}$. Equations similar to Eq. (12) have been used in earlier studies to account for carbon concentration in austenite as a function of volume fraction. According to Bhadeshia and Edmonds [31], the variation of carbon content of austenite may

be given as

$$X_\gamma = \overline{X} + f\frac{(\overline{X} - S)}{(1-f)} \tag{14}$$

where S is the fraction of carbon trapped in bainite either in solid solution (S = 0.03 wt-%) or in the form of carbides (fixed S depending on heat treatment). The term S is equivalent to the term X_b that is used in the current model. Since in a generalised model it is difficult to predict the degree of carbon enrichment or carbide precipitation, an unknown value X_b is used rather than a priori chosen value S.

Under the assumption of a displacive mechanism for bainite formation, the nucleation in bainitic ferrite is considered to occur by spontaneous dissociation of dislocations with an activation energy inversely proportional to the magnitude of driving force [17]. Thus, the activation energy can be expressed as a function of the driving force which in turn is a function of undercooling [32]. This yields

$$Q_G^* = Q_{G\overline{X}}^* + K_\Gamma C_1 \frac{f(\overline{X} - X_b)}{(1-f)} \tag{15}$$

where $Q_{G\overline{X}}^*$ is the activation energy for grain-boundary nucleation at the start of the transformation ($f = 0$; $X_\gamma = \overline{X}$) and K_Γ parameter is the proportionality constant relating activation energy for bainite nucleation and temperature. K_Γ parameter is also affected by carbon enrichment of austenite. However, calculations indicated that these effects do not significantly alter the final results. Therefore, they are neglected during further calculations.

2.4. Remaining available austenite

As seen in Eq. (9) and Eq. (11), the fraction of remaining available austenite, f_γ, is important to estimate the density of potential nucleation sites. f_γ is a fraction of the total untransformed austenite in which bainite formation can proceed. Due to carbon enrichment of austenite during the course of transformation, some fraction of austenite may not participate in the bainite reaction. This unavailable fraction of austenite would not contain any potential nucleation sites which will lead to new nucleation events and this fraction needs to be subtracted while calculating the overall nucleation rate. In this work, the unavailable austenite, $(f_\gamma)_u$, is defined as the fraction of austenite in which bainite formation cannot occur due to its stabilization by means of carbon enrichment.

Using the principles of incomplete reaction phenomenon, the T_0' curve can be used to estimate the total fraction of unavailable austenite at a particular transformation temperature with the help of the lever rule [3] (Fig. 2). The T_0' temperature decreases with increasing carbon content in austenite, as does the T_h temperature. The decrease of T_0' temperature can be expressed similar to Eq. (13) as

$$T_0' = T_{0\overline{X}}' - C_2\frac{f(\overline{X} - X_b)}{(1-f)} \tag{16}$$

where $T_{0\overline{X}}'$ is the T_0' temperature at the beginning of the transformation ($f = 0$, $X_\gamma = \overline{X}$) and C_2 is a proportionality constant relating T_0' and carbon content.

With the help of Fig. 2, it can be noticed that during transformation, the carbon enrichment leads to decrease in T_0' temperature which increases the fraction of unavailable austenite. When is equal to the isothermal transformation temperature, all the remaining austenite would stay untransformed. The fraction of unavailable austenite, $(f_\gamma)_u$, at a given point during transformation can be expressed as a function of remaining austenite fraction and the changes in T_0' temperature due to carbon enrichment, by

$$\left(f_\gamma\right)_u = (1-f)\left(\frac{T_{0\overline{X}}' - T_0'}{T_{0\overline{X}}' - T}\right) \tag{17}$$

The remaining available fraction of austenite, f_γ, at a given point during transformation can be expressed as

$$f_\gamma = 1 - f - \left(f_\gamma\right)_u \tag{18}$$

With the help of Eq. (17) and Eq. (18), f_γ can be given as

$$f_\gamma = (1-f)\left(\frac{T_0' - T}{T_{0\overline{X}}' - T}\right) \tag{19}$$

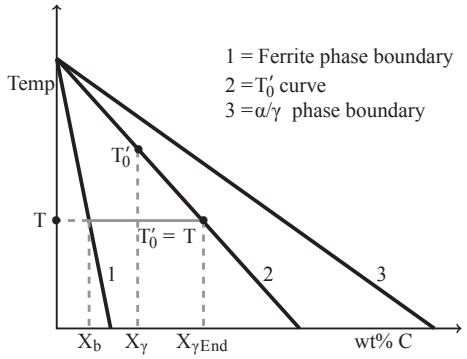

Fig. 2. Schematic diagram representing lever rule for calculation using T_0' curve.

2.5. Kinetic equation of the model

With the help of Eqs. (3)–(19), the framework of the proposed kinetic model is given here. The overall nucleation rate can be given as

$$\frac{dN}{dt} = (1-f)\left(\frac{T_0' - T}{T_{0\overline{X}}' - T}\right)\left[1 + \exp\left(\frac{\Delta Q^*}{kT}\right)f\right]\kappa \tag{20}$$

where κ is

$$\kappa = \frac{kT}{h}\frac{Z\delta}{d}\frac{m}{V_b}(T_h - T)\exp\left(-\frac{Q_G^*}{kT}\right) \tag{21}$$

T_h, Q_G^* and T_0' can be tracked using Eq. (13), Eq. (15) and Eq. (16) respectively.

X_b, $Q_{G\overline{X}}^*$ and ΔQ^* are the fitting parameters in this model. As discussed earlier, X_b is always in the range of 0 to $\overline{X}$. Literature review suggests that $Q_{G\overline{X}}^*$ is generally in the range of 150–200 kJ/mol [15]. Since all the fitting parameters used in this model can be related to a physical entity, their values can be evaluated for their physical significance (see Section 3.2.1 and Section 3.2.2).

The constants $T_{h\overline{X}}$, $T_{0\overline{X}}'$, C_1 and C_2 are calculated using Thermo-Calc. K_Γ and m are calculated using empirical methods proposed by Van Bohemen [32] and [33] respectively.

With the help of Eq. (20), the rate of bainite formation can be calculated using

$$\frac{df}{dt} = \frac{dN}{dt} V_b \tag{22}$$

Eq. (20) is very similar to the expression of nucleation rate proposed in the early works such as [12,21,22]. However, one of the major differences is that almost all the empirical constants have been replaced with physical parameters, especially the autocatalytic parameter. Earlier models of bainite kinetics based on displacive theory account for autocatalytic nucleation using the factor $(1 + \beta f)$ where β is the autocatalytic parameter. Comparing this with Eq. (20), it can be seen that

$$\beta = \exp\left(\frac{\Delta Q^*}{kT}\right) \tag{23}$$

With the use of ΔQ^*, the acceleration of bainite kinetics due to autocatalysis can be interpreted in terms of difference in activation energy for grain-boundary nucleation and autocatalytic nucleation. The carbon-enrichment dependent parameters have also been treated in such a way that bainite kinetics regardless of the chemical composition of the steel can be estimated.

3. Results and discussion

3.1. Comparison with experimental data

The proposed model was tested in a comparison with experimental data published in the literature. One of the main objectives of this work was to develop a unified model to predict isothermal transformation kinetics regardless of the degree of carbon enrichment of austenite. Therefore, kinetic data obtained from a high silicon as well as a low silicon steel were used to test the model. The chemical composition of the steels are given in Table 1.

The values for the various constants used to test the model are given in Table 2. They were obtained using Thermo-Calc as well as different empirical equations, as mentioned in Section 2.5. The prior austenite grain size in case of Steel A was 140 μm [11] while the prior austenite grain size in case of Steel B was 22 μm [16].

The experimental as well as calculated kinetics of Steel A are given in Fig. 3. The experimental kinetic data of Steel A was obtained from Ref. [11]. Fig. 4 gives the experimental and calculated kinetics of Steel B. The experimental kinetic data of Steel B was obtained from Ref. [16].

Figs. 3 and 4 shows that the model correlates well with the experimentally obtained kinetics regardless of the chemical composition of the steel.

3.2. Model fitting parameters

3.2.1. Carbon content in bainite

Carbon content in bainite, X_b, is an extremely important parameter. X_b gives a measure of the carbon redistribution during the course of the bainite formation. It influences the transformation significantly by affecting the values of T_h temperature (Eq. (13)), T'_0 temperature (Eq. (16)), activation energy (Eq. (15)), maximum volume fraction of bainite obtainable and the degree of the carbide precipitation.

From Eqs. (13), (15) and (16), it can be seen that the influence of X_b always depends on the volume fraction of bainite, f. As f increases, the influence of X_b also increases. This implies that X_b plays a greater role during the bainite formation than at the start of the transformation.

As discussed earlier, based on the degree of carbon redistribution, the value of X_b would lie in a specific range. Although an exact definition for bainite is still being debated, bainite can be viewed as an aggregate of bainitic ferrite and carbides [9]. Therefore, X_b reflects both the carbon in bainitic ferrite and the carbon in the carbides. If carbon is completely partitioned from bainitic ferrite into austenite during transformation, then X_b would be equal to 0. However, the value of X_b would never reach zero due to the solid solubility of carbon in bainitic ferrite. As the degree of carbide

Table 1
Chemical compositions of steels used for study (values in wt%).

Steel	C	Mn	Si	Cr	Al	Reference
Steel A	0.53	0.69	–	0.28	0.03	[11]
Steel B	0.3	2.4	1.8	–	–	[16]

Table 2
Values for the constants used.

	Steel A	Steel B
$T_{h\bar{X}}$	876 K	872 K
C_1	2629 K/at.fr	2926 K/at.fr
$T_{0\bar{X}}$	784 K	822 K
C_2	7196.8 K/at.fr	7353.9 K/at.fr
K_Γ	163.6 J/mol K	138.6 J/mol K
m	0.016/K	0.019/K

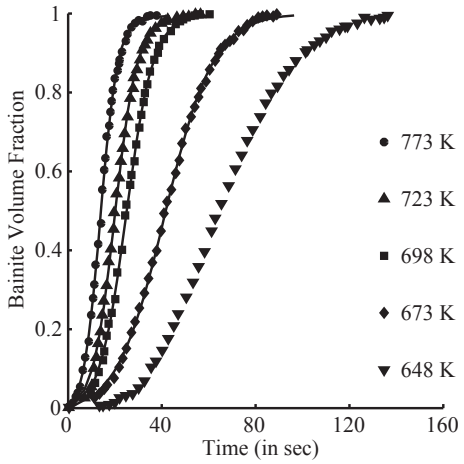

Fig. 3. Experimental [11] (markers) and calculated kinetics (solid lines) of Steel A.

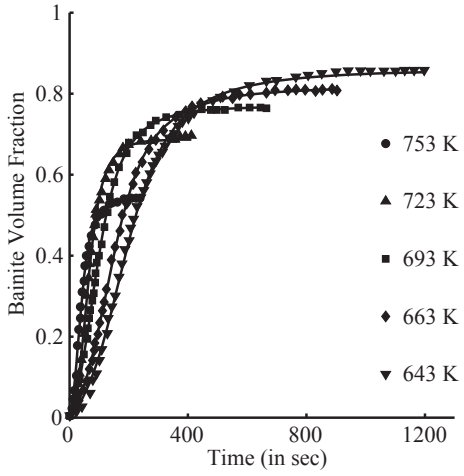

Fig. 4. Experimental [16] (markers) and calculated kinetics (solid lines) of Steel B.

precipitation increases, the value of X_b also increases. The maximum value for X_b would be $\overline{X}$. When $X_b = \overline{X}$, X_γ would also be equal to $\overline{X}$. Using lever rule (Fig. 2), it can be noticed that 100% bainite formation would occur in this case.

Due to the importance of X_b, the fit values obtained for X_b must be validated properly. The carbide precipitation in Steel A is not suppressed because of the absence of silicon. This results in negligible carbon enrichment of austenite and, as the experimental data suggests, the transformation continues until all the austenite is transformed. Based on the experimental data, the model yields that X_b is equal to the bulk carbon content of the steel at all temperatures (Table 3).

According to the displacive nature of bainite formation, an isothermal bainite reaction can proceed if and only if the T_h and T_0' temperatures are greater than the isothermal transformation temperature [20]. Eq. (13) indicates that, since X_b is equal to the bulk carbon content of the steel, the T_h temperature does not decrease during the course of the transformation. Similarly, T_0' also does not decrease which is accounted for using Eq. (16). Thus, T_h and T_0' temperatures are always greater than the isothermal transformation temperature and the bainite reaction terminates only when the austenite is consumed entirely.

Since X_b also accounts for the carbon in carbides, the value of X_b can be used as an indicator for the degree of carbide precipitation. A high X_b value suggests that the driving force for carbide precipitation during bainite formation is high. In case of Steel A, this is kinetically achievable in the absence of silicon.

Unlike Steel A, Steel B is a high silicon steel and exhibits incomplete reaction phenomenon due to the suppression of carbide precipitation. As expected, the model indicates that the X_b value is much lower than the bulk carbon concentration of the steel. The X_b values obtained for different isothermal transformations are given in Table 4. From Table 4, it can be observed that the X_b value increases with decreasing isothermal transformation temperature. Similar trend is reported in Van Bohemen and Hanlon [16]. Such a trend is due to the increase in the driving force for carbide precipitation as temperature decreases, as indicated by the phase diagram as well. This suggests that the effect of silicon on carbide suppression decreases with decreasing transformation temperature. Therefore, X_b can be used as a guideline to measure the effectiveness of silicon to precipitation of carbides.

Fig. 5 gives the comparison between experimentally obtained values and calculated values for carbon content in austenite at the end of the transformation. Fig. 5 shows that the modelled values for carbon concentration in austenite at the end of the transformation increase with decreasing isothermal temperature. Furthermore, it can be observed that the modelled values for carbon concentration in austenite at the end of the transformation is mostly lower than the experimentally observed values [16]. The experimentally observed values were obtained using XRD technique [16] which estimated the carbon content in retained austenite. Since Steel B exhibits incomplete reaction phenomenon, the untransformed austenite at the end of the bainite reaction may further transform into martensite while cooling to room temperature. This is also reported in Ref. [16]. This results in further enrichment of austenite.

Table 3
X_b values obtained for Steel A ($\overline{X}$ (in at. fr) = 0.0241).

T (in K)	X_b (in at. fr)
648	0.0240
673	0.0241
698	0.0241
723	0.0240
773	0.0241

Table 4
X_b values obtained for Steel B ($\overline{X}$ (in at. fr) = 0.0135).

T (in K)	X_b (in at. fr)
643	0.0095
663	0.0084
693	0.0083
723	0.0075
753	0.0052

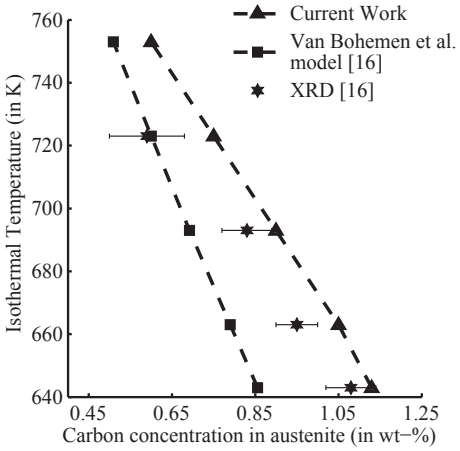

Fig. 5. Carbon concentration in austenite at the end of the transformation in Steel B.

The values calculated by the model give the carbon concentration in austenite before the martensite transformation and thus can be expected to be lower than the experimentally observed values.

The obtained X_b values indicate that the T_h and T_0' temperatures decrease during the course of transformation. The model suggests that the bainite reaction stops when the T_0' temperature reaches the isothermal transformation temperature.

3.2.2. Initial grain boundary activation energy and difference in activation energy

As discussed in Section 2.5, the activation energy for grain-boundary nucleation at the start of the transformation ($f = 0$, $X_\gamma = \overline{X}$), $Q^*_{G\overline{X}}$, as well as the difference in activation energy for grain-

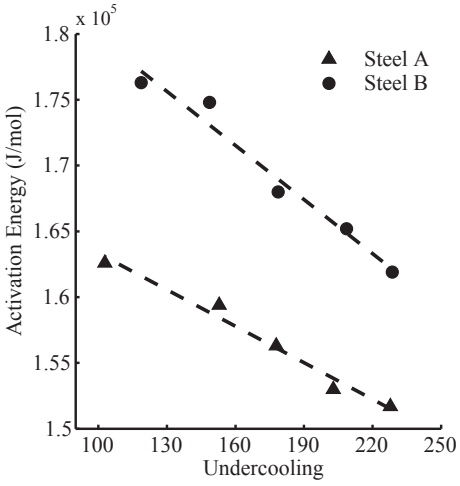

Fig. 6. Activation energy for grain-boundary nucleation at the start of transformation ($Q^*_{G\overline{X}}$) as a function of undercooling.

boundary nucleation and autocatalytic nucleation, ΔQ^*, are used as fitting parameters in the model.

In Fig. 6, $Q^*_{G\overline{X}}$, which was extracted from the fits, is plotted as a function of undercooling. Similarly, the activation energy for autocatalytic nucleation at the start of the transformation ($f = 0$, $X_\gamma = \overline{X}$), $Q^*_{A\overline{X}}$, (using Eq. (6)) is plotted as a function of undercooling in Fig. 7. In both instances, the undercooling is with respect to the T_h temperature. It can be seen that for Steel A and Steel B, both activation energies decrease linearly with undercooling. Similar trend was reported by Van Bohemen and Sietsma [15]. However, they did not distinguish between the activation energy for grain boundary and autocatalytic nucleation and considered an equal activation energy for both types of nucleation.

The linear trend observed for activation energy vs. undercooling plots in Figs. 6 and 7 suggests that thermally activated migration of partial dislocations plays an important role in bainite nucleation [17,32]. This phenomenon is irrespective of the interface at which the nucleation takes places. Therefore, both the activation energy for grain-boundary nucleation and the activation energy for autocatalytic nucleation will decrease linearly. This is observed from the fit values obtained. This generates good confidence in the trends obtained for the fit parameters as well as in the model itself.

Although the concept of direct proportionality of activation energy is used in the model to account for the changes in the activation energy during the transformation due to carbon enrichment of austenite (Eq. (15)), it does not affect the fit values obtained. The fit values only represent the activation energies at the start of the transformation ($f = 0$, $X_\gamma = \overline{X}$) and are not affected by the carbon-enrichment dependent constraints imposed by the model.

Such a dislocation motion assisted nucleation mechanism was proposed in the 1970s to explain the martensitic nucleation process [34,35]. According to this mechanism, a nucleus is formed by a faulting process derived from already existing dislocations [34–36]. The fault energy associated with the formation of a BCC nucleus in a FCC matrix depends on the change in chemical free energy due to the nucleation process, the strain energy required to accommodate the nucleus within the matrix and the nucleus/matrix interfacial energy [36]. The activation energy for the formation of the nucleus arises from the resistance to dislocation motion. Olson and Cohen [36] suggested that the activation energy is dependent on the fault energy. A decrease in the fault energy would result in a decrease in activation energy. Literature indicates that the above considerations can be extrapolated to bainite nucleation [3,14,15]. As undercooling increases, the magnitude of chemical free change during nucleation also increases which leads to a decrease in the fault energy (and consequently, activation energy).

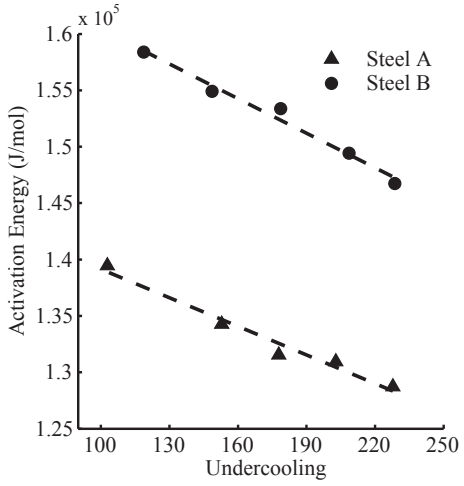

Fig. 7. Activation energy for autocatalytic nucleation at the start of transformation ($Q^*_{A\overline{X}}$) as a function of undercooling.

Literature also suggests that during bainite nucleation, carbon will partition from the BCC nucleus into FCC matrix [3,22,20]. Along with undercooling, this carbon partitioning during nucleation also leads to increase in the chemical free change. Therefore, it can be argued that carbon partitioning also leads to decrease in the overall activation energy. However, if both dislocation motion and carbon partitioning occur during nucleation, the total activation energy for nucleation may be the sum of the individual activation energies required for both processes.

The numerical values for activation energy obtained in Figs. 6 and 7 were compared with already published results. The reported values for overall activation energy for bainite formation lie in the range of 40–200 kJ/mol [15,37]. The activation energy values obtained in the current work (130–175 kJ/mol) correlates well with these reported values.

Furthermore, the activation energy values for nucleation obtained in the current work was also compared with reported activation energy values for various atomic processes [37]. The self-diffusion activation energy of Fe in α-Fe and in γ-Fe is around 250 kJ/mol and 285 kJ/mol respectively [37]. These values are much higher than the activation energy values obtained in the current work. However, the diffusion activation energy of carbon in γ-Fe is about 130 kJ/mol [37]. Comparing this value to the activation energy obtained in the current work, it can be suggested carbon diffusion in austenite plays a part in bainite nucleation. This correlates well with the above described theory of carbon partitioning during bainite nucleation. Also, assuming that the total activation energy for nucleation is the sum of activation energy for carbon partitioning and dislocation migration, the maximum expected activation energy contribution of the latter should be around 30–40 kJ/mol.

Researchers have also studied the activation energy required for dislocation movement assisted nucleation in isothermal martensite formation [38]. These studies suggest that a temperature dependent activation energy value of 29–145 kJ/mol can be expected for the migration of dislocations [38]. This range numerically compares well with the expected maximum activation energy of 30–40 kJ/mol obtained in the current work. However, it must be noted that isothermal martensite formation occurs under conditions which are vastly different from bainite formation. Therefore, numerical comparison of activation energy values must be done with caution. But, as explained above, the linearly decreasing trend observed for activation energy with undercooling is a compelling factor to consider thermally activated migration of partial dislocations as a mechanism for bainite nucleation.

Figs. 6 and 7 suggest that $Q^*_{A\overline{X}}$ is lower than $Q^*_{G\overline{X}}$. ΔQ^* for Steel A was calculated to be in the range of 22–26 kJ/mol while ΔQ^* for Steel B was estimated to be in the range of 15–20 kJ/mol.

This difference in activation energies can be attributed to the difference in resistance offered to dislocation motion in case of grain-boundary and autocatalytic nucleation as the interface at which respective nucleation events occur are different. Assuming that the shape of the nucleus formed during both grain-boundary nucleation and autocatalytic nucleation is the same, the strain energy contribution to the fault energy would the same in both cases. Also, since the degree of carbon enrichment at the start of the transformation ($f = 0$, $X_\gamma = \overline{X}$) is zero, the chemical free energy contribution is equal for grain-boundary and autocatalytic nucleation processes. However, the interfacial energy contribution is influenced by the matrix which surrounds the nucleus. In case of grain-boundary nucleation at a γ/γ interface, the entire matrix

which surrounds the nucleus is FCC, which results in the creation of α/γ interfaces between the nucleus and the matrix. However, in case of autocatalytic nucleation at an α/γ interface, both BCC (already formed bainitic ferrite sub-unit) and FCC (untransformed austenite surrounding the bainitic ferrite sub-unit) phases form the matrix in which the nucleus evolves. Nucleation then leads to the creation of both α/γ interfaces and α/α interfaces. Therefore, it can be established that, due to effects of interfacial energy contributions, the fault energy of the nucleus formed at a γ/γ interface can be expected to be different compared to that of a nucleus formed at an α/γ interface; and consequently the activation energy will also be different. Furthermore, the lower activation energy for autocatalytic nucleation may be due to the formation of low-energy interfaces during autocatalytic nucleation. Martensite nucleation theory suggests that the α/γ interfaces formed during nucleation are semi-coherent [35]. If the α/α interfaces which form during autocatalytic nucleation are more coherent than the α/γ interfaces, their contribution to the interfacial energy would be lower [39]. However, the role of 'prior' interfaces (like γ/γ interfaces) must also be taken into account while calculating the net interfacial energy. This depends on the size and the orientation of the forming nucleus.

Comparing Figs. 6 and 7, it can be noticed that the activation energy values for both mechanisms obtained for Steel A are lower than the values obtained for Steel B. This shows that the activation energy is dependent on the chemical composition of the steel. Literature suggests that the activation energy depends on both composition-dependent and composition-independent factors [32,36]. Van Bohemen [32] derived an empirical relationship to calculate the influence of steel composition on the activation energy. It is given as

$$Q_b = 89x_C + 10x_{Mn} + 12x_{Si} + 2x_{Cr} + 1x_{Ni} + 29x_{Mo} \quad (24)$$

where x_i is concentration of element i in weight percent and Q_b is a part of the overall activation energy in kJ/mol.

Using Eq. (24), the difference between the Q_b values for Steel A and Steel B is calculated to be around 18 kJ/mol. This is comparable with the activation energy values obtained from the model (Figs. 6 and 7). This indicates that the presence of manganese and silicon in steel would make the transformation slower. This can also be seen by comparing the time scales for transformation in Figs. 6 and 7.

The slopes of Figs. 6 and 7 give the K_Γ parameter. K_Γ parameter gives relationship between activation energy and temperature. As discussed in Section 2.5, this parameter is used in the model to track the changes in activation energy due to carbon enrichment. The K_Γ parameter is a material parameter and depends on the chemical composition of the steel and its chemical free energy energy contribution per Kelvin [32]. Assuming that the chemical free energy contribution is same for both mechanisms, K_Γ parameter is considered to be equal for both grain-boundary nucleation and autocatalytic nucleation. An empirical method proposed by Van Bohemen [32] is used to calculate its value. An estimated error of 9 J/mol K is associated with this empirical value. The calculated values are compared with the slopes from Figs. 6 and 7 in Table 5.

The fit values from Table 5 indicate that the K_Γ parameter for grain-boundary nucleation is not equal to K_Γ parameter for autocatalytic nucleation. Furthermore, the values obtained from the fit do not correspond well with values calculated empirically. Therefore, further investigation into the K_Γ parameter needs to be carried out.

Table 5
Comparison of K_Γ parameter (Values in J/mol K).

Steel	Empirical value	Nucleation mechanism	
		Grain-boundary	Autocatalytic
Steel A	164	93	85
Steel B	139	137s	102

An initial analysis into the physical significance of the K_Γ parameter is discussed in Ref. [32]. According to [32], using the work published by Olson and Cohen on dislocation movement assisted nucleation [36], K_Γ can be given as

$$K_\Gamma = \rho v^*/bD_T \quad (25)$$

where ρ is density of atoms in a close packed place per unit area, b is the Burgers vector associated with the existing dislocation and D_T is the proportionality constant relating driving force and undercooling. v^* is called the activation volume and it is defined as rate of change of activation energy with respect to the applied stress [36]. In the context of dislocation movement assisted nucleation, the applied stress comes from the available driving force for nucleation [3]. This suggests that the K_Γ parameter is proportional to the activation volume, v^*. The difference in K_Γ values for grain-boundary nucleation and autocatalytic nucleation may be attributed to the difference in activation volume for the two nucleation processes. A deeper understanding regarding the role of activation volume in individual nucleation processes is necessary.

However, despite the variations in the values for K_Γ parameter, they do not significantly affect the trends obtained from the model. Also, the K_Γ parameter is used in the model only to account for the variation in activation energy with composition. It does not affect the activation energy at the start of the transformation, which is a fitting parameter. The fitting parameters are independent of the constraints imposed to account for variations in activation energy due to carbon enrichment of austenite during the transformation.

4. Conclusions

A model is proposed for the prediction of isothermal bainite formation kinetics distinguishing the activation energy for grain-boundary nucleation and for autocatalytic nucleation. The model uses three fit parameters, namely carbon concentration in bainite, the activation energy for grain-boundary nucleation at the start of the transformation and the difference in activation energies for grain-boundary nucleation and autocatalytic nucleation. Furthermore, the model accounts for the variation in carbon content of austenite during the transformation. The model was tested for two different steels with different chemical compositions.

Based on the results of the tests, the traditional autocatalytic parameter may be expressed as a difference in activation energies related to the site of bainitic nucleation events. This essentially suggests that the autocatalytic parameter is a measure which indicates how much easier the autocatalytic nucleation is compared to the grain-boundary nucleation. This measure can be well represented by assuming that the activation energy for nucleation at an austenite grain boundary is much higher compared to the activation energy for nucleation at the surface of a previously nucleated bainitic sub-unit. From above discussions, it is clear that the bainite kinetics can be well predicted and interpreted with the help of this approach.

Acknowledgements

The research leading to these results has received funding from the European Research Council under the European Union's Seventh Framework Programme (FP/2007–2013)/ERC Grant Agreement n. [306292].

The authors would also like to thank Pina Mecozzi, Richard Huizenga and Stefan van Bohemen (Tata Steel RD&T) for their assistance with some calculations during this research work.

References

[1] E.S. Davenport, E.C. Bain, Transformation of austenite at constant subcritical temperatures, Metall. Trans. 1 (1970) 3503–3530.
[2] M. Hillert, Discussion of "a personal commentary on transformation of austenite at constant subcritical temperatures", Metall. Mater. Trans. A 42 (2011) 541–542.
[3] H.K.D.H. Bhadeshia, Bainite in Steels: Transformations, Microstructure and Properties, Matsci Series, IOM Communications, 2001.
[4] L.C.D. Fielding, The bainite controversy, Mater. Sci. Technol. 29 (2013) 383–399.
[5] H.K.D.H. Bhadeshia, D.V. Edmonds, The mechanism of bainite formation in steels, Acta Metall. 28 (1980) 1265–1273.
[6] W.T. Reynolds Jr., H.I. Aaronson, G. Spanos, A summary of the present diffusionist views on bainite, Mater. Trans. JIM 32 (1991) 737–746.
[7] Z.-G. Yang, H.-S. Fang, An overview on bainite formation in steels, Curr. Opin. Solid State Mater. Sci. 9 (2005) 277–286.
[8] H.K.D.H. Bhadeshia, J.W. Christian, Bainite in steels, Metall. Trans. A 21 (1990) 767–797.
[9] R.F. Hehemann, K.R. Kinsman, H.I. Aaronson, A debate on the bainite reaction, Metall. Trans. 3 (1972) 1077–1094.
[10] M. Hillert, The nature of bainite, ISIJ Int. 35 (1995) 1134–1140.
[11] D. Quidort, Y.J.M. Brechet, A model of isothermal and non isothermal transformation kinetics of bainite in 0.5% C steels, ISIJ Int. 42 (2002) 1010–1017.
[12] G.I. Rees, H.K.D.H. Bhadeshia, Bainite transformation kinetics part 1 modified model, Mater. Sci. Technol. 8 (1992) 985–993.
[13] M. Takahashi, Recent progress: kinetics of the bainite transformation in steels, Curr. Opin. Solid State Mater. Sci. 8 (2004) 213–217.
[14] M.J. Santofimia, F.G. Caballero, C. Capdevila, C. Garcia-Mateo, C.G. de Andres, New model for the overall transformation kinetics of bainite. Part 1: the model, Mater. Trans. 47 (2006) 2465–2472.
[15] S.M.C. van Bohemen, J. Sietsma, Modeling of isothermal bainite formation based on the nucleation kinetics, Int. J. Mater. Res. 99 (2008) 739–747.
[16] S.M.C. van Bohemen, D.N. Hanlon, A physically based approach to model the incomplete bainitic transformation in high-Si steels, Int. J. Mater. Res. 103 (2012) 987–991.
[17] M.J. Santofimia, F.G. Caballero, C. Capdevila, C. Garcia-Mateo, C.G. de Andres, Evaluation of displacive models for bainite transformation kinetics in steels, Mater. Trans. 47 (2006) 1492–1500.
[18] H.K.D.H. Bhadeshia, The bainite transformation: unresolved issues, Mater. Sci. Eng. A 273–275 (1999) 58–66.
[19] D. Gaude-Fugarolas, P.J. Jacques, A new physical model for the kinetics of the bainite transformation, ISIJ Int. 46 (2006) 712–717.
[20] H.K.D.H. Bhadeshia, A rationalisation of shear transformations in steels, Acta Metall. 29 (1981) 1117–1130.
[21] H.K.D.H. Bhadeshia, Bainite: overall transformation kinetics, J. de Phys. 43 (1982) 443–448.
[22] N.A. Chester, H.K.D.H. Bhadeshia, Mathematical modelling of bainite transformation kinetics, J. Phys. IV Fr. 07 (1997) 41–46.
[23] C. Garcia-Mateo, H. Bhadeshia, Nucleation theory for high-carbon bainite, Mater. Sci. Eng. A 378 (2004) 289–292 (European Symposium on Martensitic Transformation and Shape-Memory).
[24] D. Quidort, Y. Brechet, Isothermal growth kinetics of bainite in 0.5% C steels, Acta Mater. 49 (2001) 4161–4170.
[25] Z.-W. Hu, G. Xu, H.-J. Hu, L. Wang, Z.-L. Xue, In situ measured growth rates of bainite plates in an Fe-C-Mn-Si superbainitic steel, Int. J. Miner. Metall. Mater. 21 (2014) 371–378.
[26] A. Ali, H.K.D.H. Bhadeshia, Growth rate data on bainite in alloy steels, Mater. Sci. Technol. 5 (1989) 398–402.
[27] S.R. Pati, M. Cohen, Nucleation of the isothermal martensitic transformation, Acta Metall. 17 (1969) 189–199.
[28] C.L. Magee, The nucleation of martensite, in: Phase Transformation: Papers Presented at a Seminar of the American Society of Metals Oct 12 and 13, 1968, 1968.
[29] D.P. Koistinen, R.E. Marburger, A general equation prescribing the extent of the austenite-martensite transformation in pure iron-carbon alloys and plain carbon steels, Acta Metall. 7 (1959) 59–60.
[30] E. Kozeschnik, H.K.D.H. Bhadeshia, Influence of silicon on cementite precipitation in steels, Mater. Sci. Technol. 24 (2008) 343–347.
[31] H.K.D.H. Bhadeshia, D.V. Edmonds, Bainite in silicon steels: new composition – property approach part 1, Metal Sci. 17 (1983) 411–419.
[32] S.M.C. van Bohemen, Modeling start curves of bainite formation, Metallurgical Mater. Trans. A 41 (2010) 285–296.
[33] S.M.C. van Bohemen, Bainite and martensite start temperature calculated with exponential carbon dependence, Mater. Sci. Technol. 28 (2012) 487–495.
[34] G.B. Olson, M. Cohen, A general mechanism of martensitic nucleation: part I. General concepts and the FCC → HCP transformation, Metall. Trans. A 7 (1976a) 1897–1904.
[35] G.B. Olson, M. Cohen, A general mechanism of martensitic nucleation: part II. FCC → BCC and other martensitic transformations, Metall. Trans. A 7 (1976b) 1905–1914.
[36] G.B. Olson, M. Cohen, A general mechanism of martensitic nucleation: part III. Kinetics of martensitic nucleation, Metall. Trans. A 7 (1976c) 1915–1923.
[37] M. Kang, M.-X. Zhang, F. Liu, M. Zhu, Kinetics and morphology of isothermal transformations at intermediate temperature in 15CrMnMoV steel, Mater. Trans. 50 (2009) 123–129.
[38] D.S. Martin, K. Aarts, P. Rivera-Diaz-del-Castillo, N. van Dijk, E. Bruck, S. van der Zwaag, Isothermal martensitic transformation in a 12Cr-9Ni-4Mo-2Cu stainless steel in applied magnetic fields, J. Magn. Magn. Mater. 320 (2008) 1722–1728.
[39] D.A. Porter, K.E. Easterling, Phase Transformations in Metals and Alloys, Chapman and Hall, 1992.